Journal of Chromatography A, 1218 (2011) 3476–3488

Contents lists available at ScienceDirect

Journal of Chromatography A

journal homepage: www.elsevier.com/locate/chroma

# Theoretical investigation of diffusion along columns packed with fully and superficially porous particles

Fabrice Gritti, Georges Guiochon*

*Department of Chemistry, University of Tennessee, Knoxville, TN 37996-1600, USA*

ARTICLE INFO

*Article history:*
Received 9 December 2010
Received in revised form 23 March 2011
Accepted 28 March 2011
Available online 6 April 2011

*Keywords:*
Axial dispersion
Column technology
Core–shell particles
Longitudinal diffusion term
Extra-column effects

ABSTRACT

Chromatographic columns packed with shell particles are now nearly twice more efficient than columns packed with conventional, fully porous particles. Shell particles are made of a solid core surrounded by a porous shell of constant thickness. Diffusion through the bed of packed columns is complex due to their heterogeneity. It involves diffusion through the external and the internal fluid, and surface diffusion. Six diffusion models are compared that combine these diffusion mechanisms. They involve the external porosity of the bed ($\epsilon_e$), the ratio of the core to the particle diameters ($\rho$), and the ratio of the shell diffusivity to the bulk diffusion coefficient ($\Omega$). Four different theoretical approaches were considered. They are based on (1) the additivity of the mass flux densities modulated by the obstruction factors caused by non-porous spherical inclusions; (2) the effective medium theory of Landauer; (3) the effective medium theory of Garnett for spherical inclusions; and (4) the probabilistic theory of Torquato (for binary composite materials only). The two Landauer models fail because they cannot account for the obstruction factor imposed by the presence of non-porous spherical inclusions. The ternary Garnett model (3) provides an excellent approximation of the actual diffusion mechanism but the most physically relevant model seems to be the one derived from a combination of the Garnett model for a binary core–shell particle and of the Torquato model for random dispersion of contacting spheres in a matrix. Accurate measurements of axial dispersion coefficients are needed to validate or reject the semi-empirical parallel diffusion models and to select the most appropriate one. The results of such measurements made with the peak parking method for various compounds are reported in the companion paper.



## 1. Introduction

The recent production of columns packed with sub-3 μm core–shell particles has attracted considerable attention in industrial and academic laboratories [1–20]. No fewer than three manufacturers are now competing to provide such packing materials including Halo (Advanced Material Technologies, Wilmington, DE, USA), Kinetex (Phenomenex, Torrance, CA, USA), and Poroshell120 (Agilent Technologies, Little Falls, DE, USA). At least two academic groups are developing similar materials [21,22]. The performance of these columns is now equivalent to that of columns packed with sub-2 μm particles over which they have the important advantages of requiring markedly lower operating pressures and exhibiting lesser efficiency loss due to thermal effects at high flow rates [10,12,13]. For instance, a 4.6 mm I.D. column packed with Kinetex 2.6 μm could generate corrected plate counts as large as 320 000 plates/m [10].

The original perceived incentive that drove the introduction of core–shell particles was the expectation that the diffusion path across the shells of these particles being shorter would lead to a flatter *C* branch of the van Deemter kinetic plot and higher column efficiencies at high flow velocities. Admittedly, theoretical investigations of the apparent diffusivity of analyte molecules through commercial core–shell particles, with a ratio of their core to particle diameters ranging between 0.63 and 0.73 predict a reduction by a factor 2 of the reduced trans-particle mass transfer coefficient, $C_p$ [23–25]. In fact, however, $C_p$ does not control the mass transfer kinetics of small molecules at high velocities because the HETP contribution of $C_p\nu$ is too small, except possibly for large biomolecules.

Comparisons between columns packed with shell and with fully porous particles have unambiguously demonstrated that the exceptional performance of the former columns is due to the low contributions of both eddy diffusion (reduced *A* term) and longitudinal diffusion (reduced $B/\nu$ term) to band broadening in these columns. The reasons for the unusually low value of the *A* term of columns packed with shell particles is still unknown. It could be explained either by the tight particle size distribution of the shell particles (ca. 5%) and/or by the small trans-column velocity biases in columns packed with them. The origin for the decrease of the *B* coef-

* Corresponding author. Tel.: +1 865 974 0733; fax: +1 865 974 2667.
*E-mail address:* guiochon@utk.edu (G. Guiochon).

0021-9673/$ – see front matter © 2011 Elsevier B.V. All rights reserved.
doi:10.1016/j.chroma.2011.03.063

ficient is simpler: 20% of the column volume is occupied by the solid, nonporous, spherical silica cores, through which analyte molecules cannot diffuse. Additionally, the presence of these cores induce a degree of obstruction to the diffusion of these molecules. Knox and McLaren [26] built a three-dimensional model of nonporous spheres, which predicts a nearly linear increase of the obstruction factor from 0.57 to unity when the bed porosity increases from 0.33 (spheres in contact) to 1.0 (no sphere). For a porosity of 80%, this model predicts an obstruction factor of 0.87. However, the prediction of accurate values of the $B$ coefficient proves complex. Most models of effective diffusion proposed so far for packed LC columns [27] are valid only for binary composite materials and cannot fully account for the complex micro-structure of chromatographic beds packed with core–shell particles. The primary goal of our work is to propose and discuss new models of effective diffusion for these beds.

In this work, we investigate the rigorous derivation of a physically consistent model of the effective diffusion coefficient, $D_{eff}$, in heterogeneous media made of three different phases. This model should account for the contributions of the nonporous cores, the porous shells, and the eluent impregnating a chromatographic column packed with core–shell particles. We assume that core and shells are concentric and that the spherical particles are in contact and randomly packed inside the column filled of eluent. Simple models are currently used in chromatography and the standard parallel diffusion model is often found in the chromatography literature [28]. A more sophisticated model was derived from the effective medium theory of Landauer [29], adapted to diffusion by Davis [30] for ternary composite materials. We will show how to build more appropriate diffusion models by combining the Garnett [31] and the Torquato [32] diffusion models. The former model, based on perturbation theory, provides the effective diffusion coefficient of spherical core–shell inclusions. The latter model, based on the stochastic theory [33], provides the effective diffusion coefficient for a bed of spheres in contact but randomly dispersed in a matrix. The designs of these two models are such that they should afford the "exact" effective diffusion coefficient in chromatographic columns packed with shell particles. Accordingly, these models should predict how the ratio of analyte diffusivities in the core and in the eluent varies with the ratio of the core to the particle diameters.

## 2. Theory

This section lists models of equivalent diffusion in composite materials that could potentially account for the longitudinal diffusion term of the van Deemter plots of chromatographic columns packed with spherical core–shell particles. All these models are discussed in terms of their physical relevance with respect to the actual distribution of the superficially porous particles inside a packed bed. For all models, the bed is assumed to be a ternary composite medium made of spherical cores, concentric spherical shells, and a homogeneous surrounding matrix (the eluent).

We first consider the general case in which the cores can be porous and permeable, and the concentrations in the cores, in the concentric shells, and in the surrounding matrix are $c_1$, $c_2$, and $c_3$, respectively. The diffusion coefficients in each of these phase are defined as $D_1$, $D_2$, and $D_3$. Accordingly, the local mass flux density, $\vec{j}_i$, in phase $i$ is written:

$$\vec{j}_1 = -D_1 \vec{\nabla} c_1 \tag{1}$$

$$\vec{j}_2 = -D_2 \vec{\nabla} c_2 \tag{2}$$

$$\vec{j}_3 = -D_3 \vec{\nabla} c_3 \tag{3}$$

where $\vec{\nabla} c_i$ is the local concentration gradient of the analyte in the homogeneous phase $i$. Additionally, it is assumed that all three phases are in thermodynamic equilibrium, with the equilibrium constant $K_1$ and $K_2$ being:

$$K_1 = \frac{c_1}{c_2} \tag{4}$$

$$K_2 = \frac{c_2}{c_3} \tag{5}$$

The volume fractions occupied by the three phases are $\phi_1$, $\phi_2$, and $\phi_3$, with:

$$\phi_1 + \phi_2 + \phi_3 = 1 \tag{6}$$

The goal of our work is the derivation of an expression of the equivalent or effective diffusion coefficient, $D_{eff}$, of the heterogeneous medium as a function of $D_1$, $D_2$, $D_3$, $K_1$, $K_2$, $\phi_1$, and $\phi_2$. At a scale significantly larger than that of the particle size, the effective mass flux density is:

$$\vec{j}_{eff} = -D_{eff} \vec{\nabla} c_{eff} \tag{7}$$

where the effective concentration, $c_{eff}$, is the average concentration of the analyte considered measured over a scale far larger than the size of the local micro-heterogeneities:

$$c_{eff} = \phi_1 c_1 + \phi_2 c_2 + \phi_3 c_3 = [1 + \phi_1(K_1 K_2 - 1) + \phi_2(K_2 - 1)]c_3 \tag{8}$$

In this work, we study a steady-state problem, assuming that the mass flux densities are constant everywhere in the system at both macroscopic and microscopic scales. For the sake of simplicity, apply to the composite material a constant concentration gradient, $\vec{\nabla} c_{eff}$, along the $x$-axis, i.e., placing the macroscopic system in an homogeneous field, $\vec{E}$, equal to the opposite of the "potential" gradient:

$$\vec{E} = -\vec{\nabla} c_{eff} = -E_0 \vec{i} \tag{9}$$

where $\vec{i}$ is the unit vector directed from the region of low towards the region of high concentrations. The positive and constant parameter $E_0$ measures the constant rate at which the effective concentration increases linearly along the $x$-axis. The divergence of this field is obviously zero ($div\vec{E} = 0$) so the Laplacian of the effective concentration is zero everywhere:

$$\Delta c_{eff} = 0 \tag{10}$$

Under steady-state condition there is no accumulation of mass and this conclusion is also true at a microscopic scale in each homogeneous phase $i$ and:

$$\Delta c_1 = 0 \tag{11}$$

$$\Delta c_2 = 0 \tag{12}$$

$$\Delta c_3 = 0 \tag{13}$$

### 2.1. The parallel diffusion model

In the parallel diffusion model, it is assumed that the effective flux density of mass is the volume average of the microscopic flux densities. Therefore,

$$\vec{j}_{eff} = \phi_1 \vec{j}_1 + \phi_2 \vec{j}_2 + \phi_3 \vec{j}_3 \tag{14}$$

$$\vec{j}_{eff} = -\frac{\phi_1(K_1 K_2 D_1 - D_3) + \phi_2(K_2 D_2 - D_3) + D_3}{1 + \phi_1(K_1 K_2 - 1) + \phi_2(K_2 - 1)} \vec{\nabla} c_{eff} \tag{15}$$

The comparison of Eqs. (7) and (14) shows that $D_{eff}$ is equal to:

$$D_{eff} = \frac{\phi_1(K_1 K_2 D_1 - D_3) + \phi_2(K_2 D_2 - D_3) + D_3}{1 + \phi_1(K_1 K_2 - 1) + \phi_2(K_2 - 1)} \tag{16}$$

#### 2.1.1. Binary mixtures

For binary composite materials ($\phi_1 = 0$), Eq. (16) becomes:

$$D_{eff} = \frac{\phi_2(K_2 D_2 - D_3) + D_3}{1 + \phi_2(K_2 - 1)} \tag{17}$$

This model ignores the physical obstruction of axial diffusion that takes place if phase 2 is partially or fully impermeable. This can be *a posteriori* corrected by replacing the diffusion coefficient $D_3$ with an apparent diffusion coefficient $\gamma_3 D_3$, where $\gamma_3$ account for the obstruction generated by material 2. Later, in Section 3, we will assess $\gamma_3$ for partially permeable spheres based on the work of Knox and McLaren [26].

#### 2.1.2. Ternary mixture

For ternary composite materials with impermeable cores ($D_1 = K_1 = 0$), Eq. (16) is written:

$$D_{eff} = \frac{-\phi_1 D_3 + \phi_2(K_2 D_2 - D_3) + D_3}{1 - \phi_1 + \phi_2(K_2 - 1)} \tag{18}$$

The major advantage of the parallel diffusion model is its great simplicity. Its downside is that it ignores the actual spatial distribution of the different phases involved in the packed bed (randomly packed core–shell particles in contact, immersed in the bulk liquid phase). This model ignores the obstructions due to both the impermeable phase 1 and the partially permeable phase 2. Again, *a posteriori*, $D_3$ and $D_2$ can be replaced by $\gamma_3 D_3$ (obstruction due to the partial permeability of the spherical phase 2) and $\gamma_2 D_2$ (obstruction due to the complete impermeability of the spherical phase 1). In Section 3, we will assess $\gamma_2$ for fully impermeable spheres according to the work of Garnett [31]. More sophisticated models of effective diffusion are thus needed. Next, we investigate the results obtained based on the classical effective medium theory of Landauer.

### 2.2. The Landauer effective medium theory

Landauer elaborated a self-consistent effective medium theory of conductivity [29] in order to account for the influence on this conductivity of the inclusion of local heterogeneities in materials of practical relevance. Later, Davis showed that the solution for diffusion should obey the following general relationship [30,34]:

$$\sum_i \phi_i \frac{D_i c_i - D_{eff} c_{eff}}{D_i c_i + 2D_{eff} c_{eff}} = 0 \tag{19}$$

where $i$ runs over the number of homogeneous phases in the mixture.

#### 2.2.1. Binary mixtures

For a binary mixture, assume $\phi_1 = 0$ (no solid core). Eq. (19) writes:

$$\phi_2 \frac{D_2 c_2 - D_{eff} c_{eff}}{D_2 c_2 + 2D_{eff} c_{eff}} + (1 - \phi_2) \frac{D_3 c_3 - D_{eff} c_{eff}}{D_3 c_3 + 2D_{eff} c_{eff}} = 0 \tag{20}$$

This second order polynomial has only one physically meaningful solution, its positive root:

$$D_{eff} = \frac{a_{bin} + \sqrt{a_{bin}^2 + (1/2)(D_2/D_3)K_2}}{1 + \phi_2(K_2 - 1)} D_3 \tag{21}$$

with

$$a_{bin} = \frac{1}{4}\left[2 - 3\phi_2 + \frac{D_2}{D_3} K_2 (3\phi_2 - 1)\right] \tag{22}$$

#### 2.2.2. Ternary mixture

In the presence of a solid core, the bed becomes a ternary mixture and Eq. (19) writes:

$$\phi_1 \frac{D_1 c_1 - D_{eff} c_{eff}}{D_1 c_1 + 2D_{eff} c_{eff}} + \phi_2 \frac{D_2 c_2 - D_{eff} c_{eff}}{D_2 c_2 + 2D_{eff} c_{eff}} + (1 - \phi_1 - \phi_2) \frac{D_3 c_3 - D_{eff} c_{eff}}{D_3 c_3 + 2D_{eff} c_{eff}} = 0 \tag{23}$$

Eq. (19) has always a positive root for $D_{eff}$, which is the unique solution of the physical problem. The general explicit formulation is too long to be written here but it can easily be calculated numerically. Interestingly, a simple solution can be derived for impermeable cores ($D_1 = K_1 = 0$). The positive root is written:

$$D_{eff} = \frac{a_{ter} + \sqrt{a_{ter}^2 + (1/2)(1 - (3/2)\phi_1)(D_2/D_3)K_2}}{1 - \phi_1 + \phi_2(K_2 - 1)} D_3 \tag{24}$$

with

$$a_{ter} = \frac{1}{4}\left[2 - 3\phi_1 - 3\phi_2 + \frac{D_2}{D_3} K_2 (3\phi_2 - 1)\right] \tag{25}$$

The weakness of the effective medium theory of Landauer is the same as that of the parallel diffusion model: the lack of consideration of the specific spatial distribution of the three homogeneous phases in the chromatographic column. Its advantage is that it provides an obstruction factor and imposes no constraints regarding the combination (parallel or series) of the local mass flux densities $j_i$. In the next section, we derive a model of effective diffusivity for a composite material made exclusively of a solid core surrounded by either one or two concentric spherical shells.

### 2.3. The Garnett approach for effective diffusivity in core–shell particles

In this section, we apply the approach developed by Garnett [31] to assess the effective diffusivity of spherical core–shell particles and that of a bed of core–shell particles immersed in a homogeneous matrix.

#### 2.3.1. Binary mixture: one concentric shell

Consider the general case of a binary mixture made of an homogeneous phase 1 (diffusion coefficient $D_1$, concentration $c_1$, volume fraction $\phi_1$) dispersed in a homogeneous phase 2 (diffusion coefficient $D_2$, concentration $c_2$, and volume fraction $1 - \phi_1$). At the macroscopic scale, this material appears to be homogeneous and has an effective diffusion coefficient $D_{eff}$ and a concentration $c_{eff}$. $D_{eff}$ is an unknown function of $D_1$, $D_2$, and $\phi_1$. It also depends on the geometry of phase 1 dispersed in phase 2, which we define next.

Suppose now that we extract a sphere of radius $r_2$ from this effective medium and replace it with a sphere made of a spherical core of radius $r_1$ composed of a first homogeneous material 1 surrounded by a spherical shell of radius $r_2$ made of a second homogeneous material, 2. The ratio $r_1/r_2$ is chosen so that it matches exactly the volume fraction $\phi_1$ in the previous binary mixture or $r_1^3/r_2^3 = \phi_1$.

The unknown effective diffusion coefficient, $D_{eff}$, in the effective medium made of such a core–shell binary composite material is obtained from the following physical argument that the introduction of the core–shell particles just described does not modify the concentration profile in the volume external to these particles, which is controlled by the imposed concentration gradient along the composite material (Eq. (8)). In the steady-state regime, Eqs. (10) and (11) apply and should be resolved exactly by taking into account the symmetry of the diffusion problem in the spherical core and in the surrounding concentric shell and the Laplacian of the local concentration in spherical coordinates (the radius $r$, the angle

$\theta$ between the invariant concentration field gradient $\vec{E}$ and the vector position $\vec{r}$, and the azimutal angle $\varphi$). Since we are interested in situations with axial symmetry around the vector $\vec{E}$, the local concentration, $c_i$, in phase $i$ is only a function of the coordinates $r$ and $\theta$. Therefore, the steady state equation is written:

$$\frac{\partial}{\partial r}\left(r^2\frac{\partial c_i}{\partial r}\right)+\frac{1}{\sin\theta}\frac{\partial}{\partial\theta}\left(\sin\theta\frac{\partial c_i}{\partial\theta}\right)=0 \tag{26}$$

The general solution to this differential equation is given in mathematical textbooks by a linear combination of Legendre polynomials in cos $\theta$ or:

$$\begin{aligned}c_i(r,\theta)&=\sum_{k=0}^{k=\infty}\left(A_{i,k}r^k+\frac{B_{i,k}}{r^{k+1}}\right)P_k(\cos\theta)\\&=\left(A_{i,0}+\frac{B_{i,0}}{r}\right)+\left(A_{i,1}r+\frac{B_{i,1}}{r^2}\right)\cos\theta\\&+\left(A_{i,2}r^2+\frac{B_{i,2}}{r^3}\right)(3\cos^2\theta-1)+\left(A_{i,3}r^3+\frac{B_{i,3}}{r^4}\right)\\&\times(5\cos^3\theta-3\cos\theta)+\cdots\end{aligned} \tag{27}$$

where $A_{i,k}$ and $B_{i,k}$ are integration constants, and $k$ ($0<k<\infty$) is the order of the Legendre polynomial.

The actual concentration profiles are simple, however, given the physical constraints that the profiles should fulfil in certain regions of the space. First, the concentration in the spherical core (material 1, $r<r_1$) is finite at $r=0$. Therefore, for any integer $k$ in the general expression of $c_i(r,\theta)$, $B_{1,k}=0$. Second, we assumed that the concentration gradient along the direction $\vec{i}$ is linear, so, for all $k>1$, $A_{1,k}=0$. By convention let assume that $c_1(0,\theta)=0$ so that $A_{1,0}=0$. Accordingly, the sample concentration profile in the core made of material 1 reduces to:

$$c_1(r,\theta)=A_{1,1}r\cos\theta \quad r<r_1 \tag{28}$$

Second, the concentration profile in the effective medium surrounding the core–shell particle, $c_{eff}$, is known. It was imposed by the uniform field of concentration gradients along the $x$-axis. Therefore:

$$c_{eff}(r,\theta)=E_0r\cos\theta \quad r>r_2 \tag{29}$$

Finally, the concentration profile in the shell made of material 2 surrounding the core is given in its more general form by:

$$c_2(r,\theta)=\left(A_{2,1}r+\frac{B_{2,1}}{r^2}\right)\cos\theta \quad r_1<r<r_2 \tag{30}$$

All the other coefficients $A_{2,k}$ and $B_{2,k}$ are equal to zero because the solution of the problem is symmetrical, due to the linear concentration gradient along the $x$-axis ($x=r\cos\theta$).

In conclusion, we are left with four unknowns: the three integration constants $A_{1,1}$, $A_{2,1}$, and $B_{2,1}$ and the effective diffusivity $D_{eff}$, which is the unknown that is really sought after. Adequate boundary conditions are needed to find these four constants.

*2.3.1.1. Boundary conditions.* First, we assume that phases 1 and 2 are in thermodynamic equilibrium everywhere. Therefore, at $r=r_1$ and $r=r_2$, we have for all $\theta$:

$$c_1(r_1,\theta)=K_1c_2(r_1,\theta) \tag{31}$$

or

$$r_1^3A_{1,1}-K_1r_1^3A_{2,1}-K_1B_{2,1}=0 \tag{32}$$

and

$$c_2(r_2,\theta)=\frac{1}{1+\phi_1(K_1-1)}c_{eff}(r_2,\theta) \tag{33}$$

or

$$r_2^3A_{2,1}-\frac{E_0}{1+\phi_1(K_1-1)}r_2^3+B_{2,1}=0 \tag{34}$$

Eqs. (32) and (34) account for the discontinuity in the concentrations at the boundaries between the different homogeneous phases.

Second, under steady-state conditions, the mass flux density remains continuous from one phase to another (since there is no mass accumulation). For all $\theta$, the following conditions should be fulfilled:

$$D_1\frac{\partial c_1(r,\theta)}{\partial r}|_{r_1}=D_2\frac{\partial c_2(r,\theta)}{\partial r}|_{r_1} \tag{35}$$

or

$$r_1^3D_1A_{1,1}-r_1^3D_2A_{2,1}+2D_2B_{2,1}=0 \tag{36}$$

and

$$D_2\frac{\partial c_2(r,\theta)}{\partial r}|_{r_2}=D_{eff}\frac{\partial c_{eff}(r,\theta)}{\partial r}|_{r_2} \tag{37}$$

or

$$r_2^3D_2A_{2,1}-r_2^3D_{eff}E_0-2D_2B_{2,1}=0 \tag{38}$$

*2.3.1.2. Solution.* Eqs. (32), (34), (36) and (38) form a $4\times4$ matrix system $[M][X]=[Y]$. The elements $m_{ij}$, $x_{i,1}$, and $y_{i,1}$ are as follows:

$$\begin{bmatrix}r_1^3 & -r_1^3K_1 & -K_1 & 0\\ 0 & r_2^3 & 1 & 0\\ r_1^3D_1 & -r_1^3D_2 & 2D_2 & 0\\ 0 & r_2^3D_2 & -2D_2 & -r_2^3E_0\end{bmatrix}\begin{bmatrix}A_{1,1}\\A_{2,1}\\B_{2,1}\\D_{eff}\end{bmatrix}=\begin{bmatrix}0\\E_0r_2^3\\1+\phi_1(K_1-1)\\0\\0\end{bmatrix}$$

The inverse matrix $[M]^{-1}$ is needed to solve the problem $[X]=[M]^{-1}[Y]$. The calculation was performed using Maple 7.0 software, giving $x_{4,1}=D_{eff}(D_1,D_2,\phi_1)$ from the product $m_{4,2}^{-1}\times y_{2,1}$ or:

$$D_{eff}=\frac{D_2}{1+\phi_1(K_1-1)}\frac{2D_2+D_1-2\phi_1(D_2-K_1D_1)}{2D_2+D_1+\phi_1(D_2-K_1D_1)} \tag{39}$$

*2.3.2. Ternary mixture: two concentric shells*

The problem is similar to the previous one, but with the addition of a second spherical shell surrounding the first one. Three radii are then defined, $r_1$, $r_2$, and $r_3$ (see Fig. 1). The purpose is to account

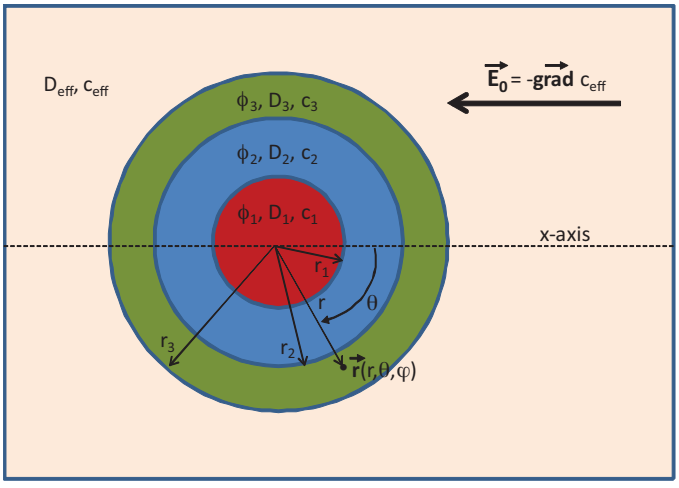


**Fig. 1.** Insertion in a composite medium of a spherical inclusion made of a sphere (radius $r_1$) surrounded by two concentric shells (between radii $r_1$ and $r_2$, and $r_2$ and $r_3$). The constant concentration gradient imposed to the composite material is shown by the thick solid arrow. The effective diffusion coefficient, $D_{eff}$, of the spherical inclusion is found by considering that its insertion does not change the concentration gradient anywhere in the composite medium surrounding the inclusion.

for diffusion through the whole volume of a chromatographic bed packed with particles which have a non-porous core, a first concentric shell made of porous silica and a second concentric shell made of the bulk eluent.

Accordingly, a third phase is introduced and the concentration profile in this second shell is written:

$$c_3(r,\theta) = \left(A_{3,1}r + \frac{B_{3,1}}{r^2}\right)\cos\theta \quad r_2 < r < r_3 \tag{40}$$

Two new integration constants ($A_{3,1}$ and $B_{3,1}$) appear but also two new boundary conditions, between the two concentric shells (phase 2 and phase 3) at $r = r_2$. They are written

$$c_2(r_2,\theta) = K_2 c_3(r_2,\theta) \tag{41}$$

or

$$r_2^3 A_{2,1} - K_2 r_2^3 A_{3,1} + B_{2,1} - K_2 B_{3,1} = 0 \tag{42}$$

and

$$D_2 \frac{\partial c_2(r,\theta)}{\partial r}|_{r_2} = D_3 \frac{\partial c_3(r,\theta)}{\partial r}|_{r_2} \tag{43}$$

or

$$r_2^3 D_2 A_{2,1} - r_2^3 D_3 A_{3,1} - 2D_2 B_{2,1} + 2D_3 B_{3,1} = 0 \tag{44}$$

The system of 6 equations and 6 unknowns form a $6 \times 6$ matrix system $[M][X] = [Y]$. The elements $m_{ij}$, $x_{i,1}$, and $y_{i,1}$ are:

$$\begin{bmatrix} r_1^3 & -r_1^3K_1 & -K_1 & 0 & 0 & 0 \\ 0 & r_2^3 & 1 & -r_2^3K_2 & -K_2 & 0 \\ 0 & 0 & 0 & r_3^3 & 1 & 0 \\ r_1^3D_1 & -r_1^3D_2 & 2D_2 & 0 & 0 & 0 \\ 0 & r_2^3D_2 & -2D_2 & -r_2^3D_3 & 2D_3 & 0 \\ 0 & 0 & 0 & r_3^3D_3 & -2D_3 & -r_3^3E_0 \end{bmatrix} \begin{bmatrix} A_{1,1} \\ A_{2,1} \\ B_{2,1} \\ A_{3,1} \\ B_{3,1} \\ D_{eff} \end{bmatrix}$$

$$= \begin{bmatrix} 0 \\ 0 \\ \dfrac{E_0 r_3^2}{1-\phi_1+\phi_2(K_2-1)} \\ 0 \\ 0 \\ 0 \end{bmatrix}$$

Again, the inverse matrix $[M]^{-1}$ was obtained using the Maple 7.0 software. If phase 1 is impermeable ($D_1 = K_1 = 0$), we can determine $D_{eff}(D_2, D_3, \phi_1, \phi_2, K_2)$ from the product $m_{6,3}^{-1} \times y_{3,1}$ or:

$$D_{eff} = \frac{D_3}{1-\phi_1+\phi_2(K_2-1)} \frac{D_3(6\phi_1+4\phi_2-6\phi_1^2-4\phi_2^2-10\phi_1\phi_2)+2\phi_2K_2D_2(1+2\phi_2+2\phi_1)}{D_3(6\phi_1+4\phi_2+3\phi_1^2+2\phi_2^2+5\phi_1\phi_2)+2\phi_2K_2D_2(1-\phi_2-\phi_1)} \tag{45}$$

It is easy to check that when $\phi_2$=0, the diffusion problem is equivalent to that of a binary mixture with an impermeable core.

The advantage of the model illustrated by Eq. (45) is that it takes into account the spatial distribution of the solid non-porous core ($\phi_1$), the porous shell ($\phi_2$), and the eluent ($1-\phi_1-\phi_2$) embedding the core–shell particles. The downside of this model is the weak representation of the interstitial volume geometry in an actual packed chromatographic column.

### 2.4. The Torquato's effective diffusion model

The previous models of effective conductivity are based on the hypothesis of the additivity of the contributions of the different phases involved (Section 2.1), on the classical Landauer model [29] of inclusions occupying a certain volume fraction (see Section 2.2), and on the model of Garnett [31] in which the spherical inclusions are embedded in a concentric spherical matrix (Section 2.3). These models are approximate. More elaborate models were derived based on the known microstructural details of the composite medium [33]. They are based on the probability ($n$-point probability function) of finding in a point of space either one of the different homogeneous phases that make the whole composite medium. For instance, in the case of the random dispersion of impenetrable spheres of conductivity $\sigma_2$ in a matrix of conductivity $\sigma_3$, some effective electrical conductivity were approximated to a second order expression as [32]:

$$\frac{\sigma_{eff}}{\sigma_3} = \frac{1+2\phi_2\beta-2(1-\phi_2)\xi_2\beta^2}{1-\phi_2\beta-2(1-\phi_2)\xi_2\beta^2} \tag{46}$$

where

$$\beta = \frac{\sigma_2-\sigma_3}{\sigma_2+2\sigma_3} \tag{47}$$

and $\xi_2$ is the so-called three-point parameter for randomly distributed impenetrable spheres. $\xi_2 = 0.3277$ when $\phi_2 = 0.60$, e.g., when the spheres are typically close to be in contact. Such expression have been reported recently in the field of chromatography [27] to solve the problem of mass diffusion. According to the general notations defined in this work, Eq. (46) was reformulated as:

$$D_{eff} = \frac{D_3}{1+\phi_2(K_2-1)} \frac{1+2\phi_2\beta-2(1-\phi_2)\xi_2\beta^2}{1-\phi_2\beta-2(1-\phi_2)\xi_2\beta^2} \tag{48}$$

with

$$\beta = \frac{D_2K_2-D_3}{D_2K_2+2D_3} \tag{49}$$

Clearly, in the Torquato model of effective diffusivity, the presence of fully and/or superficially porous particles accounts for the composition of the homogeneous phase 2.

### 2.5. The link between $D_{eff}$ and the longitudinal diffusion coefficient in the van Deemter equation

In the previous sections, we derived and elaborated a series of equations providing the effective diffusion coefficient, $D_{eff}$, in binary and ternary composite media. These equations should allow the prediction of the actual flux of analyte molecules, $j_{eff} = D_{eff}\nabla c_{eff}$, as a function of the diffusion coefficients and the volume fractions of the homogeneous phases which constitute the composite material.

Let assume a column packed with core–shell particles. This column is made of spherical solid non-porous cores ($\phi_1$, $c_1$) surrounded by concentric porous shells ($\phi_2$, $c_2$) immersed in the mobile phase matrix ($\phi_3$, $c_3$). The mass balance equation is then written:

$$\phi_1\frac{\partial c_1}{\partial t} + \phi_2\frac{\partial c_2}{\partial t} + \phi_3\frac{\partial c_3}{\partial t} = D_{eff}\frac{\partial^2 c_{eff}}{\partial x^2} \tag{50}$$

Therefore, combining Eqs. (50) and (8) allows the derivation of the apparent axial diffusion coefficient along the column:

$$\frac{\partial c_3}{\partial t} = D_{eff}\frac{\partial^2 c_3}{\partial x^2} \tag{51}$$

The effective diffusion coefficient, $D_{eff}$, defined in this section is thus equal to the apparent diffusion coefficient, $D_{app}$, along the chromatographic column:

$$D_{eff} = D_{app} \tag{52}$$

If the reduced longitudinal diffusion term, $B$, refers to the interstitial linear velocity, $u$, it is then written [35]:

$$B = 2\left[1 + \frac{\phi_2}{1-\phi_1-\phi_2}K_2\right]\frac{D_{eff}}{D_3} \quad (53)$$

## 3. Results and discussion

In this work, we selected the models of effective diffusion coefficients which seemed to be the most suitable to account for analyte diffusion in columns packed with core–shell particles. Then, we expressed these models as functions of the bed external porosity $\epsilon_e$, the core to particle diameter, $\rho$, the diffusion coefficient in the bulk phase, $D_m$, and the effective diffusivity in the shell, $D_{shell} = \Omega D_m$, derived from the concentration gradient in the bulk phase ($j_{shell} = -D_{shell}\nabla c_m$).

On the one hand, when the model can be applied directly to diffusion problem in a ternary composite, its variables $\phi_1$, $\phi_2$, $K_2$, $D_2$, and $D_3$ will be written:

$$\phi_1 = (1-\epsilon_e)\rho^3 \quad (54)$$

$$\phi_2 = (1-\epsilon_e)(1-\rho^3) \quad (55)$$

$$K_2 = \frac{c_{shell}}{c_m} = \epsilon_p + [1-\epsilon_p]K \quad (56)$$

$$D_2 = \frac{D_{shell}}{K_2} = \frac{\Omega}{\epsilon_p + [1-\epsilon_p]K}D_m \quad (57)$$

and

$$D_3 = D_m \quad (58)$$

This applies to the parallel diffusion model Eq. (18), the Landauer diffusion model Eqs. (24) and (25), and the Garnett model Eq. (45).

On the other hand, when the model is derived from the combination of two models which both apply to binary composite materials, the effective diffusion coefficient of the core–shell particles predicted by the first model will serve for the homogeneous phase 2 of the second model. The first model is the Garnett diffusion model given by Eq. (39), which takes into account an impermeable spherical core (phase 1) surrounded by a concentric porous shell (phase 2). In order to determine the effective diffusion coefficient $D_{core-shell}$, the non zero variables $\phi_1$ and $D_2$ will be written:

$$\phi_1 = \rho^3 \quad (59)$$

and

$$D_2 = \frac{\Omega}{\epsilon_p + [1-\epsilon_p]K}D_m \quad (60)$$

The second model of this combination will be either the parallel diffusion model in Eq. (17), the Landauer diffusion model in Eqs. (21) and (22) or the Torquato's model Eqs. (48) and (49). The variables $\phi_2$, $K_2$, $D_2$, and $D_3$ in this second model of diffusion are written:

$$\phi_2 = 1-\epsilon_e \quad (61)$$

$$K_2 = \frac{c_{core-shell}}{c_m} = \frac{\rho^3 c_{core} + (1-\rho^3)c_{shell}}{c_m} = (1-\rho^3)(\epsilon_p + [1-\epsilon_p]K) \quad (62)$$

$$D_2 = D_{core-shell} \quad \text{(from previous first model)} \quad (63)$$

and

$$D_3 = D_m \quad (64)$$

The solution provides directly the apparent diffusivity (see Section 2.5) in the packed column, $D_{app}$. The $B$ term is obtained according to Eq. (53) with the parameters $\phi_1 = (1-\epsilon_e)\rho^3$, $\phi_2 = (1-\epsilon_e)(1-\rho^3)$, $K_2 = \epsilon_p + [1-\epsilon_p]K$, and $D_3 = D_m$.

So, we derived six original models of effective diffusion in chromatographic columns packed with core–shell particles, models that could potentially be introduced in the general van Deemter mass transfer equation. We discuss and compare them in terms of their ability to predict the experimental $B$ coefficients.

### 3.1. Effective diffusion coefficient of ternary composite materials based on the composition of two binary effective diffusion models

First, we determine the effective diffusion coefficient, $D_2 = D_{core-shell}$, of a core–shell particle based on the approach of Garnett with a single concentric shell.

#### 3.1.1. Model 1

From Eq. (39), we derive $D_{core-shell}$ as:

$$D_{core-shell} = \frac{1}{1+(\rho^3/2)}\frac{\Omega}{\epsilon_p + [1-\epsilon_p]K}D_m \quad (65)$$

The diffusion coefficient $D_{core-shell}$ will serve as the diffusion coefficient $D_2$ in the next three models of effective diffusion for binary composite materials.

#### 3.1.2. Model 2

*3.1.2.1. Parallel diffusion model.* Combining Eqs. (65), (17) and (53) gives the reduced longitudinal $B$ term of the column:

$$B = 2\left[\gamma_e + \frac{1-\epsilon_e}{\epsilon_e}\frac{1-\rho^3}{1+(\rho^3/2)}\Omega\right] \quad (66)$$

where $\gamma_e$ is the obstruction factor parameter which accounts for the hindrance of diffusion across the particles immersed in the eluent. It was empirically introduced because the $B$ values should satisfy the constraint that for non-porous shells ($\rho = 1$), $B = 2\gamma_e$ consistent with the obstruction to diffusion caused by fully impermeable spherical particles in a randomly packed bed [26,36,37] and $\gamma_e$ is usually taken as 0.6.

This model is called the Garnett–Parallel model. Note that this is a semi-empirical model by construction, designed to account for the diffusion hindrance in the bulk phase caused by the non-porous shells.

*3.1.2.2. Landauer diffusion model.* Combination of Eqs. (65), (21), (22) and (53) gives the reduced longitudinal $B$ coefficient of the column:

$$B = \frac{2}{\epsilon_e}\left[a_{bin} + \sqrt{a_{bin}^2 + \frac{1}{2}\frac{1-\rho^3}{1+(\rho^3/2)}\Omega}\right] \quad (67)$$

with

$$a_{bin} = \frac{1}{4}\left[3\epsilon_e - 1 + (2-3\epsilon_e)\frac{1-\rho^3}{1+(\rho^3/2)}\Omega\right] \quad (68)$$

This model is called the Garnett–Landauer model. It ignores the shape and the specific distribution of the two homogeneous phases inside the column.

*3.1.2.3. Torquato's diffusion model.* Combination of Eqs. (65), (48), (49) and (53) gives the reduced longitudinal $B$ term of the column:

$$B = \frac{2}{\epsilon_e}\left[\frac{1+2(1-\epsilon_e)\beta - 2\epsilon_e\xi_2\beta^2}{1-(1-\epsilon_e)\beta - 2\epsilon_e\xi_2\beta^2}\right] \quad (69)$$

with

$$\beta = \frac{((1-\rho^3)/(1+(\rho^3/2)))\Omega - 1}{((1-\rho^3)/(1+(\rho^3/2)))\Omega + 2} \quad (70)$$

and $\xi_2 = 0.3277$ when the inclusion (core–shell particles) are in physical contact [32].

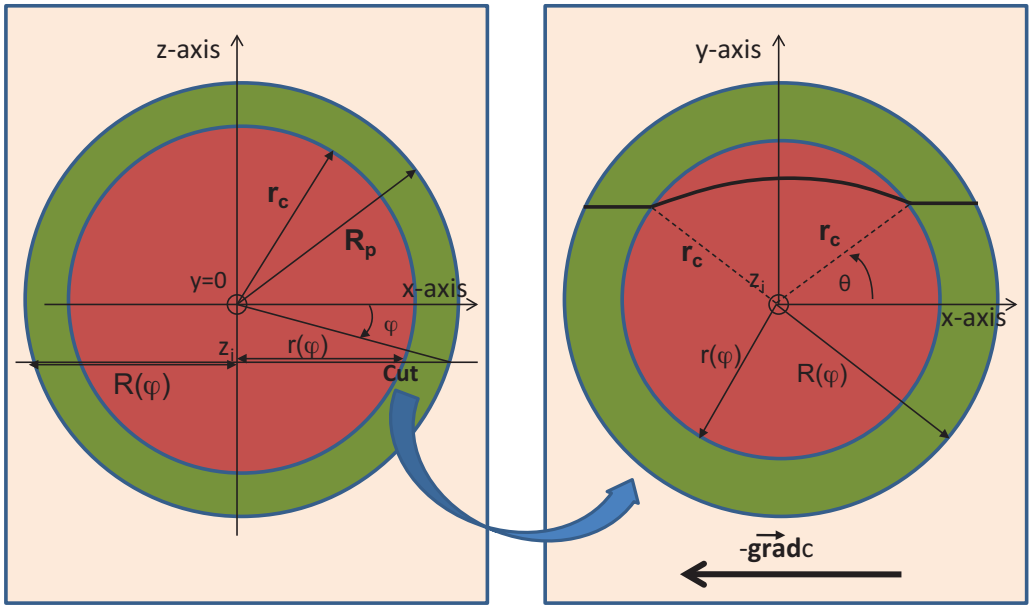


**Fig. 2.** Left: cut of the core–shell particles along the *xz*-plan. The radius of the core is $r_c$ and the radius of the particle is $R_p$. Right: cut of the core–shell particle along the *xy*-axis at $z = z_i$. The thick line is showing the tortuous diffusion path caused by the impermeable core when a concentration gradient is imposed along the *x*-axis.

This model is called the Garnett–Torquato model. This is the model most physically consistent with the actual structure of chromatographic beds, made of core–shell particles randomly packed and immersed in a bulk eluent matrix. It takes into account both the geometry of the core–shell particles (Garnett model) and their random spatial distribution inside the column (Torquato model). The only approximation of this composed model is that it does not account for the diffusion hindrance caused in the eluent bulk by the presence of the partially permeable particles.

### 3.2. Effective diffusion coefficient of ternary composite materials based on ternary effective diffusion models

#### 3.2.1. Parallel diffusion model

This model is given by Eqs. (18) and (53) in which two obstruction factors, $\gamma_e$ and $\gamma_p$, are introduced to account for the reflection of analyte molecules at the surfaces of the shell and of the impermeable cores, respectively. This model is called the Ternary–Parallel model:

$$B = 2\left[\gamma_e + \gamma_p \frac{1-\epsilon_e}{\epsilon_e}(1-\rho^3)\Omega\right] \tag{71}$$

This model is also a semi-empirical model by construction since the constraints of diffusion hindrance caused by the walls of the shell ($\gamma_e$) and the cores ($\gamma_p$) are added. In absence of cores ($\rho = 0$), $\gamma_p = 1$. As the shell thickness progressively decreases towards zero ($\rho \to 1$), the obstruction factor also decreases. But we need a model to account for the decrease of $\gamma_p$ with increasing $\rho$. We considered and compared two different models for $\gamma_p$. These models depend on the assumption made for the diffusion lines defined locally as the gradient vector of the local concentration. Note that the diffusion lines do not reflect the random trajectory of a single molecule:

- First consider an approximate a model of obstruction caused by a spherical, impermeable core of variable radius to diffusion across a core–shell particle. Consider such a particle defined by its parameter $\rho = r_c/R_p$, where $r_c$ is the radius of the core and $R_p$ the radius of the concentric shell (see left graph in Fig. 2). Let the concentration gradient be along the *x*-axis and assume for the sake of simplicity that diffusion takes place along this axis in the shell volume. When the molecules reflects against the core surface, they are forced to diffuse along an arc of radius $r_c$ along the surface of the core (see right graph in Fig. 2). In the next paragraphs we calculate the length of this diffusion line as a function of the angles $\varphi$ and $\theta$ and compare it to the length of the straight path, providing the local tortuosity factor. Integration over the whole surface area of the sphere allow us to compute an average tortuosity factor, $\tau_p$. The obstruction factor is finally obtained from the reciprocal of the average tortuosity factor squared.

Fig. 2 (right) shows a vertical cut of the core–shell particle along a *x*–*y* plane located at coordinate $z_i$ within the range $-r_c < z_i < r_c$. Out of this range, there is no reflection and the molecule is assumed to diffuse along a straight path (then local tortuosity factor is equal to unity). The intersection between the spherical core, the spherical concentric shell, and the plane $z = z_i$ generates two concentric circles of radii, $r(\varphi)$ (core) and $R(\varphi)$ (shell). Both angles, $\varphi$ and $\theta$, vary in the ranges $0 < \varphi < \pi/2$ the fraction 1/8th of the sphere surface area. By symmetry, the problem is the same in any other 1/8th of the sphere surface area.

Simple trigonometry leads to:

$$r(\varphi) = R_p\sqrt{\rho^2 - \sin^2\varphi} \tag{72}$$

and

$$R(\varphi) = R_p\cos\varphi \tag{73}$$

We may define then the new parameter $\rho(\varphi)$:

$$\rho(\varphi) = \frac{r(\varphi)}{R(\varphi)} = \frac{\sqrt{\rho^2 - \sin^2\varphi}}{\cos\varphi} \tag{74}$$

By definition, the average tortuosity factor, $\tau_p$ is calculated over 1/8th of the whole surface area of the sphere of radius $R_p$ ($dS = R_p^2\cos\varphi\, d\theta\, d\varphi$):

$$\tau_p = \frac{\int_0^{\pi/2}\int_0^{\pi/2}\tau(\varphi,\theta)\cos\varphi\, d\theta\, d\varphi}{\int_0^{\pi/2}\int_0^{\pi/2}\cos\varphi\, d\theta\, d\varphi} \tag{75}$$

The molecule is reflected by the core/shell interface and the tortuosity $\tau(\varphi, \theta)$ is different from unity when $\varphi < \arcsin\rho$ and $\theta < \arcsin\rho(\varphi)$. For any other angles, we may assume a straight

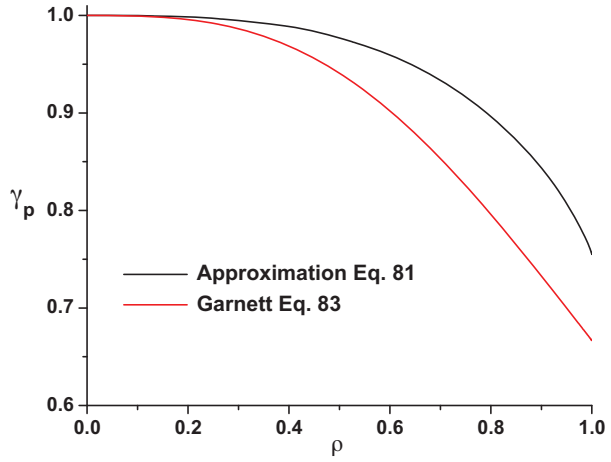


**Fig. 3.** Comparison between the two expressions of the obstruction factor, $\gamma_p$, caused by a solid non-porous core to the diffusion across a core–shell particle, assuming a uni-axial concentration gradient. Black: approximate model assuming obstruction only at the surface of the core. The diffusion lines are straight lines in the shell volume along the *x*-axis. Red: Garnett model assuming the true diffusion lines in the shell volume. (For interpretation of the references to color in this figure legend, the reader is referred to the web version of the article.)

diffusion path and $\tau_p(\varphi,\theta)=1$. Elementary trigonometric considerations, give:

$$\tau(\varphi,\theta)=1-\frac{\sqrt{\rho^2(\varphi)-\sin^2\theta}}{\cos\theta}+\frac{\rho}{\cos\varphi\cos\theta}\arccos\times\left[1-\frac{\rho^2-\sin^2\varphi}{\rho^2}\left(1-\frac{\sin\theta}{\rho(\varphi)}\right)\right] \quad (76)$$

Combining Eqs. (76) and (75) leads to the final result:

$$\tau_p=1+\frac{2}{\pi}\int_0^{\arcsin\rho}\int_0^{\arcsin\rho(\varphi)}\tau(\varphi,\theta)\cos\varphi\,d\theta\,d\varphi-\frac{2}{\pi}\int_0^{\arcsin\rho}\arcsin\rho(\varphi)\cos\varphi\,d\varphi \quad (77)$$

The tortuosity coefficient, $\tau_p$ can be easily computed from this double integral and $\gamma_p(\rho)=1/\tau_p^2(\rho)$ is plotted in Fig. 3. The limitation of this model is obvious since it ignores the true mass flux densities in the concentric shell across which diffusion flux are no longer parallel to the *x*-axis. Accordingly, this model is expected to provide a value of the obstruction factor closer to unity. Next, we estimate the true obstruction factor based on the exact concentration profile in the shell volume.

- Consider now the exact concentration profile $c(r,\theta,\rho)$ in the shell given by the inverse of the $4\times4$ matrix derived in the theory section. Taking the opposite of the gradient of $c(r,\theta,\rho)$ allows to derive the mass flux density vector $\vec{j}(r,\theta,\rho)$ everywhere in the shell:

$$\vec{j}(r,\theta,\rho)=\frac{E_0D_2}{(2+\rho^3)(1-\rho^3)}\left[-2\cos\theta\left(1-\frac{r_1^3}{r^3}\right)\vec{u}_r+\sin\theta\left(2+\frac{r_1^3}{r^3}\right)\vec{u}_\theta\right] \quad (78)$$

According to the binary Garnett model, the following obstruction factor is obtained:

$$\gamma_p(\rho)=\frac{1}{1+(\rho^3/2)} \quad (79)$$

Note that the Ternary–Parallel model is equivalent to the Garnett–Parallel model if we assume $\gamma_p$ given by Eq. (79). In Fig. 3, we compare the two different expressions of $\gamma_p$. The one derived from the Garnett approach appears to be more realistic and should be considered in the calculation of the *B* coefficient (see the model comparison in Fig. 4). The Garnett–Parallel and the Ternary–Parallel models merge into a single model of effective diffusion in packed beds.

#### 3.2.2. Landauer diffusion model

The *B* term is derived from Eqs. (24), (25) and (53):

$$B=\frac{2}{\epsilon_e}\left[a_{ter}+\sqrt{a_{ter}^2+\frac{1}{2}\left(1-\frac{3}{2}[1-\epsilon_e]\rho^3\right)\Omega}\right] \quad (80)$$

with

$$a_{ter}=\frac{1}{4}[3\epsilon_e-1+\Omega(3[1-\epsilon_e][1-\rho^3]-1)] \quad (81)$$

This model is called the Ternary–Landauer model. It provides its own obstruction factor due to the presence of the impermeable cores but ignores the geometry of the different homogeneous phases constituting the composite material (spherical cores, concentric spherical shell in contact, and surrounding eluent matrix). Only their volume fractions are relevant for the prediction of the *B* coefficient.

#### 3.2.3. Garnett diffusion model

Eq. (45) was used to give the following expression of *B*:

$$B=\frac{4}{\epsilon_e}\frac{\epsilon_e(2+\rho^3)+\Omega(1-\rho^3)(3-2\epsilon_e)}{(3-\epsilon_e)(2+\rho^3)+2\Omega(1-\rho^3)\epsilon_e} \quad (82)$$

This model is called the Ternary–Garnett model. It respects the geometry of the particles but ignores the physical contact between the packed shell particles, e.g., the spatial distribution of the bulk eluent matrix surrounding these particles. By construction, this model assumes the filling of the entire interstitial void with a series of smaller and smaller inclusions down to infinitesimally small. This model describes the *B* coefficient of a fractal composite material. However, a packed chromatographic bed is not a fractal object. Finally, this model does not take into account the diffusion hindrance in the bulk caused by the walls of the porous concentric shell.

### 3.3. Model comparison

In this section, we compare the variations with the core to particle diameter ratio, $\rho$, of the effective diffusion coefficients that are predicted by the five models described earlier and expressed by Eqs. (66), (67), (69), (80) and (82). We assume for the characteristics of the porous shell an internal porosity $\epsilon_p=0.4$, an internal obstruction factor $\gamma=0.5$, a hindrance diffusion factor $F(\lambda_m)=0.7$ [38] for small molecules, and an average mesopore size of 100 Å. Accordingly, for non-retained compound, we have $\Omega=\epsilon_p\gamma F(\lambda_m)=0.14$ [39]. We consider two cases, whether the analyte is moderately ($\Omega=1$) or strongly ($\Omega=1.5$) retained. The external porosity of the column was set at $\epsilon_e=0.4$.

#### 3.3.1. Non retained compounds

The theoretical plots of the reduced *B* term as a function of the parameter $\rho$ for a non-retained compound inform essentially on the ability of the models at predicting the degree of obstruction generated by the core of the particles when $\rho\to1$. Knox and McLaren [26,37] showed that $B=2\gamma_e\simeq2\times0.6=1.2$ for non-porous particles . Fig. 5 compares the plots of *B* versus $\rho$ provided by the five models described above. Not surprisingly, the Garnett–Parallel converges to $B=1.2$ when $\rho\to1$, because this constraint was included into the model.

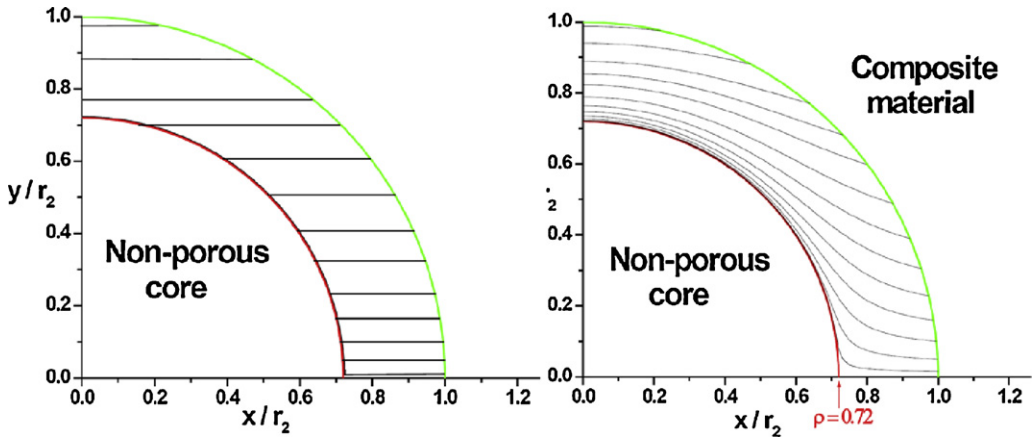


**Fig. 4.** Comparison between the diffusion trajectories assumed for the two models of tortuosity in a spherical shell surrounding a non-porous core. Left: straight diffusion trajectories assumed in the shell, until reflection from the surface of the nonporous core. Right: diffusion trajectories as described by the mass flux density vector Eq. (78) derived from the Garnett model. This second set of trajectories seems a more realistic diffusion.

Interestingly, the two Landauer models, the Garnett–Torquato model, and the Ternary–Garnett model generate different obstruction factors $\gamma_e$ for non porous particles. These factors are:

$$\gamma_e = \frac{1}{2}\frac{3\epsilon_e - 1}{\epsilon_e} = 0.25 \tag{83}$$

for the two Landauer-based models,

$$\gamma_e = \frac{2(1-(\xi_2/2))}{3-\epsilon_e(1+\xi_2)} = 0.68 \tag{84}$$

for the Garnett–Torquato model ($\xi_2 = 0.3277$), and

$$\gamma_e = \frac{2}{3-\epsilon_e} = 0.77 \tag{85}$$

for the Ternary–Garnett model. These low values of $\gamma_e$ suggest that the two Landauer models do not properly account for the actual obstruction to axial diffusion that takes place in beds packed with spherical nonporous particles. The Landauer theory does not seem to apply either at high concentrations of inclusions in the matrix. The Landauer model underestimates the value of $B$ for nonretained compounds in columns packed with shell particles at all values of $\rho$.

In contrast, the obstruction factors derived from the Garnett–Torquato (0.68) and the Ternary–Garnett (0.77) models seem to make great physical sense. They are consistent with the assumptions made in the Garnett model, in which the spatial distributions of the nonporous cores (solid sphere), the porous shells (concentric sphere), and the eluent (the surrounding matrix) is exactly (Garnett–Torquato) or nearly (Ternary–Garnett) the one that is observed in actual columns. In the Garnett–Torquato model, the particles are in contact as they are in actual packed beds. In the Ternary–Garnett model, the shells are never in contact because they are surrounded by an impenetrable concentric shell of eluent. Hence, it is not surprising to find that the obstruction factor is slightly larger in this case (0.77) than the one predicted by the Garnett–Torquato model (0.68), which accounts for the nearly constant difference ($0.10 < \Delta B < 0.16$) between the values predicted by the Ternary–Garnett and Garnett–Torquato models.

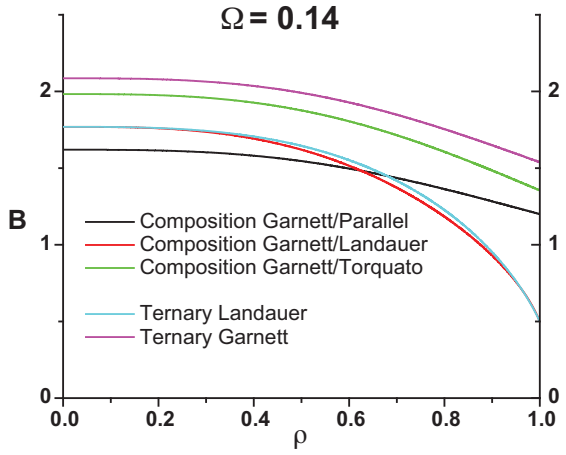


**Fig. 5.** Plot of the reduced longitudinal diffusion coefficient $B$ as a function of the ratio of the core to the particle diameter, $\rho$, for a non-retained sample and for all five models of effective diffusion coefficients in chromatographic packed with core–shell particles. The external porosity of the bed is $\epsilon_e = 0.4$ and the relative analyte diffusivity in the shell to that in the bulk phase ($D_m$), $\Omega$, is equal to 0.14.

The distinction between the Garnett–Parallel model, on the one hand, and the Garnett–Torquato and Ternary–Garnett models, on the other hand, when $\rho$ is close to 0 (fully porous particles) is easily explained. Due to the constraint imposed to the Garnett–Parallel model at $\rho = 1$, this model appears irrelevant at low $\rho$ values because the porous shell cannot be fully impermeable to the eluent. As the Landauer models, this model certainly underestimates the actual $B$ term of fully porous particles. This conclusions will be checked by comparing the predicted and the experimental values of the $B$ terms discussed in the companion paper.

The difference between the $B$ coefficients predicted by the Garnett–Torquato and the Ternary–Garnett models stems essentially from the slightly different values of the intrinsic obstruction factors that are predicted by these two models for $\rho = 1$. This difference is relatively small and is related to the physical relevance of both models.

### 3.3.2. *Moderately retained compounds*

For compounds that are moderately retained in RPLC, the parameter $\Omega$ is usually around unity. When $\Omega = 1$, the actual chromatographic column packed with core–shell particles is equivalent to a hypothetical column filled with a mobile phase in which are dispersed nonporous spherical inclusions (not in contact) the volume fraction of which varies between 0 and $1 - \epsilon_e$. Therefore, it is not surprising to see in Fig. 6 that four of the models derived in this work (the two Landauer models, the Garnett–Torquato and the Ternary–Garnett models) provide the same value for the $B$ coefficient for $\rho = 0$, e.g. when the hypothetical column is entirely filled with the pure eluent. Accordingly, the $B$ coefficient is equal to $2/\epsilon_e = 5$ for these models. Because the obstruction factor $\gamma_e$ was empirically introduced in the Garnett–Parallel model, the $B$ values predicted by this model at $\rho = 0$ is slightly smaller, equal to 4.52.

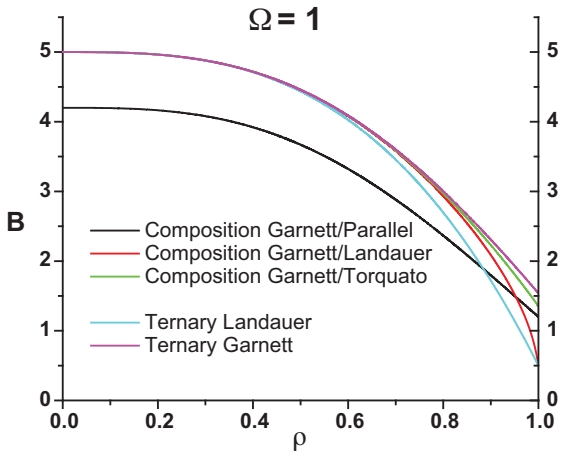


**Fig. 6.** Plot of the reduced longitudinal diffusion coefficient $B$ as a function of the ratio of the core to the particle diameter ratio, $\rho$, for a moderately retained compound in RPLC and for all five models of effective diffusion coefficients in chromatographic packed with core–shell particles. The external porosity of the bed is $\epsilon_e = 0.4$ and the relative sample diffusivity in the shell to that in the bulk phase ($D_m$), $\Omega$, is equal to 1.0.

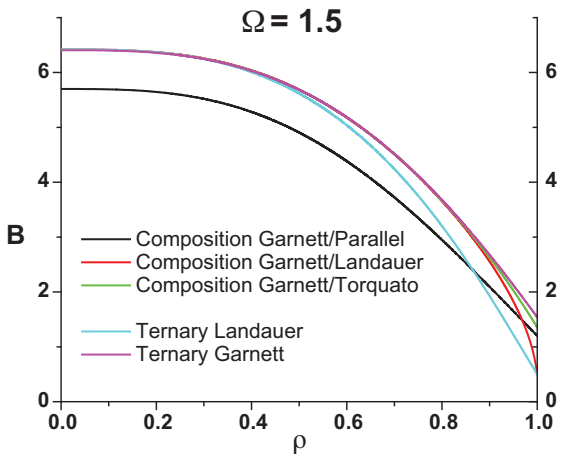


**Fig. 7.** Plot of the reduced longitudinal diffusion coefficient $B$ as a function of the ratio of the core to the particle diameter ratio, $\rho$, for a strongly retained sample in RPLC and for all five models of effective diffusion coefficients in columns packed with core–shell particles. The external porosity of the bed is $\epsilon_e = 0.4$ and the relative sample diffusivity in the shell to that in the bulk phase ($D_m$), $\Omega$, is equal to 1.5.

The trends in Fig. 6 are very close for all the models when $\rho \to 0$. However, when the shell thickness decreases ($\rho \to 1$) and the obstruction to diffusion due to the nonporous cores becomes effective, the trends of these models become noticeably different for $\rho > 0.6$. The Garnett–Parallel model predicts a nearly linear decrease of the $B$ coefficient. In contrast, the other models predict a convex upward curve, severely convex for the Landauer models and only slightly convex for the Garnett–Torquato and the Ternary–Garnett models. Therefore, accurate measurements with the peak parking method of the $B$ coefficient of moderately retained compounds on columns packed with silica-$C_{18}$ core–shell particles having values of $\rho$ in the range $0.6 < \rho < 1$ should provide a test comparing the validity of the Garnett–Parallel model (which should exhibit a nearly linear behavior) and the Garnett–Torquato and Ternary–Garnett models, which should provide a slightly convex upward behavior.

### 3.3.3. Strongly retained compounds

For strongly retained compounds, $\Omega$ can be as large as 1.5 [39,36]. For $\Omega = 1.5$, the trends remain similar to those observed in Fig. 6 but, as Fig. 7 demonstrates, it becomes difficult to distinguish between the predictions made by the three Garnett models for values of $\rho$ below ca. 0.92.

### 3.3.4. Preliminary experimental results on sub-3 μm core–shell particles

The parameter $\rho$ of the commercial 2.6 μm Kinetex, 2.7 μm Halo, and 2.7 μm Poroshell120 shell particles are equal to 0.73, 0.63, and 0.63, respectively [15]. Figs. 8 and 9 show plots of the variation of the reduced $B$ coefficients versus the parameter $\Omega$ for all five models of effective diffusion in packed beds and for two constant parameters $\rho = 0.63$ and 0.73, respectively. The shells of most particles of this type have a finite thickness and occupy typically 60–75% of the particle volume. From a physical point of view, the parameter $\Omega$ varies typically between 0 (complete exclusion from the mesoporous network of the shell for large molecular weight compounds) to 1.5 in RPLC (maximum contribution of surface diffusion of small molecules to the diffusivity in the shell [36]).

The difference between the curvatures predicted by the five models is striking for $0 < \Omega < 0.5$. As expected, the plot is strictly linear for the Garnett–Parallel diffusion model; they are severely convex upward for the two Landauer models, and only slightly so

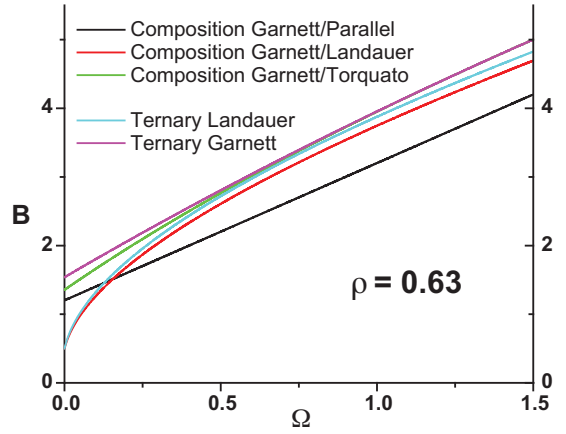


**Fig. 8.** Plot of the reduced longitudinal diffusion coefficient $B$ as a function of the ratio of the sample diffusivity in the porous shell to the bulk diffusion coefficient, $\Omega$, for 2.7 μm Halo or Poroshell120 shell particles ($\rho = 0.63$) and for all five models of effective diffusion coefficients in chromatographic packed with core–shell particles. The external porosity of the bed is $\epsilon_e = 0.4$.

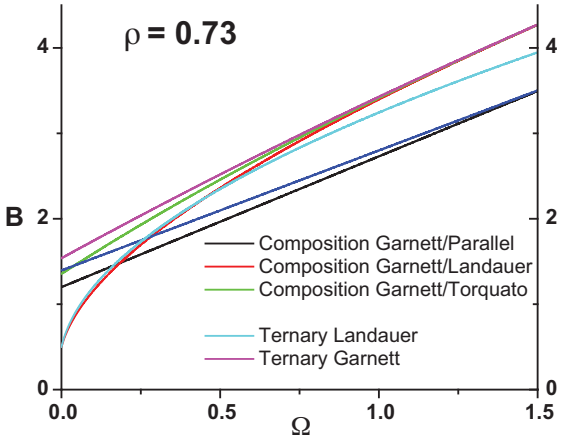


**Fig. 9.** Plot of the reduced longitudinal diffusion coefficient $B$ as a function of the ratio of the sample diffusivity in the porous shell to the bulk diffusion coefficient, $\Omega$, for 2.6 μm Kinetex shell particles ($\rho = 0.73$) and for all five models of effective diffusion coefficients in chromatographic packed with core–shell particles. The external porosity of the bed is $\epsilon_e = 0.4$.

for the Garnett–Torquato and the Ternary–Garnett models. Would the direct, independent measurement of $\Omega$ be possible, it would be easy to select the best diffusion model. Figs. 8 and 9 demonstrate why weakly retained solutes should be used in RPLC to select the preferable model of effective diffusion. The precision with which the coefficient $B$ can now be measured is certainly sufficient for this purpose.

We selected the 2.7 μm Halo 90 Å column ($L$ = 150 mm × $d_c$ = 4.6 mm), four weakly retained low molecular weight analytes (uracil, acetophenone, toluene, and naphthalene), eluted with an acetonitrile/water (80/20, v/v) solution, at room temperature $T$ = 295 K. Their bulk molecular diffusion coefficients $D_m$ were estimated from the Wilke and Chang correlation [40], giving 1.15, 1.39, 1.54, and $1.33 \times 10^{-5}$ cm$^2$/s, respectively. The peak parking method was applied in a previous work [17] in order to estimate the reduced $C_p$ coefficient of this column. The flow rate used was $F_v$ = 0.30 mL/min and the peak parking times were 1, 30, 60, 120, 240, and 480 min were selected. The external porosity of the column was $\epsilon_e$ = 0.400. The total porosity was derived from inverse size-exclusion chromatography (ISEC) measurements, by extrapolation of the elution volume of polystyrene standards to the molecular size of eluent molecules, e.g., 3.5 Å. It was found equal to $\epsilon_t$ = 0.498, giving retention factors of 0.00, 0.36, 0.99, and 1.21, respectively. The reduced $B$ coefficients were derived according to the following equation [35]:

$$B = \frac{1}{D_m}\frac{\Delta\sigma^2_{PP}}{\Delta t_p}\frac{u^2}{1+((1-\epsilon_e)/\epsilon_e)[\epsilon_p+(1-\epsilon_p)K](1-\rho^3)} \quad (86)$$

where $\Delta\sigma^2_{PP}/\Delta t_p$ is the slope of the experimental plot of the peak variance $\Delta\sigma^2_{PP}$ $v$ ersus the peak parking time $t_p$ provided by the peak parking experiments for the four compounds (0.00427, 0.01050, 0.02289, and 0.02057 s ±1%, respectively), $u = 4F_v/\epsilon_e\pi d_c^2 = 0.301$ cm/s ±0.5% is the interstitial linear velocity, $\epsilon_p = (\epsilon_t - \epsilon_e)/((1-\epsilon_e)(1-\rho^3)) = 0.218$ is the internal porosity of the porous silica-$C_{18}$ shell, and $K$ the adsorption/desorption equilibrium Henry constant in the porous shell (0.00, 0.51, 1.40, and 1.72).

This procedure provided values of $B$ equal to 1.69 (uracil), 2.52 (acetophenone), 3.40 (toluene), and 3.17 (naphthalene). The relative error made on these coefficient is ±10%, essentially due to the relative error made on estimates of the diffusion coefficients $D_m$ in Eq. (86). For the purpose of comparison, the diffusion coefficient of uracil was directly measured using the peak parking method with a column packed with non-porous particles from which we knew the external obstruction factor $\gamma_e$. A difference of +13% was measured [41].

For each diffusion model $i$, we determined the corresponding $\Omega_i$ parameters. The plots of these $\Omega_i$ parameters *versus* the experimental $B_{exp}$ coefficients are shown in Fig. 10.

The solid lines in this graph represents the expected $\Omega$ values from each theoretical model for any measurable $B$ values within the range $1.6 < B_{exp} < 3.6$ and for a constant core-to-particle diameter ratio $\rho$ = 0.63. The lowest $B$ value was 1.69 ± 10% with uracil. Given the internal porosity of the Halo-$C_{18}$ porous shell ($\epsilon_p \simeq 0.2 \pm 15\%$) and an internal obstruction factor of $\gamma(\epsilon_p) \simeq 0.4 \pm 20\%$ [42] and a diffusion hindrance factor $F(\lambda_m) \simeq 0.7 \pm 10\%$ [38], it is reasonable to expect a $\Omega$ value close to $0.06 \pm 45\%$ or $0.03 < \Omega < 0.09$. The Garnett–Parallel diffusion model predicts a $\Omega$ value of 0.24. Similar $\Omega$ values (0.20 and 0.18) were expected according to the Landauer models. In contrast, the Garnett–Landauer ($\Omega$ = 0.11) and Ternary–Landauer ($\Omega$ = 0.06) diffusion models provide $\Omega$ value in close agreement with the physical expectation.

The measurement of the $B$ coefficient of a non-retained compound demonstrates that parallel diffusion models cannot account properly for effective diffusion in packed chromatographic beds. Neither Landauer models can. The Garnett–Torquato and the Ternary–Garnett diffusion models seem to be the most suitable models of effective diffusion to account for the experimental $B$ coefficients of packed columns. This needs further experimental validation involving columns packed with core–shell particle having various $\rho$ values.

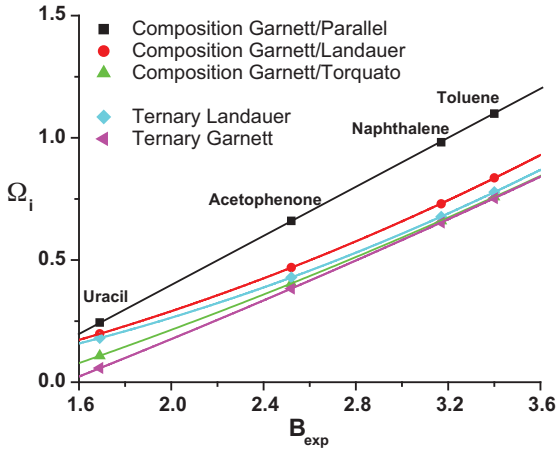


**Fig. 10.** Plot of the ratio of the sample diffusivity in the porous shell to the bulk diffusion coefficient, $\Omega_i$ (obtained from a model of diffusion $i$ as indicated in the legend of the graph) as a function of the experimental longitudinal diffusion coefficient $B_{exp}$. $\rho$ = 0.63 and the external porosity of the bed is $\epsilon_e$ = 0.4.

## 4. Conclusion

Models of diffusion were designed to predict effective diffusion coefficients of analytes in chromatographic beds made of either fully porous or core–shell particles percolated by a fluid stream. These models provide the expected variations of the classical $B$ coefficient in the classical van Deemter equation as a function of the core-to-particle diameter ratio, which varies from 0 (fully porous particle) to 1 (non-porous particles). The shell particles are made of a nonporous spherical core surrounded by a concentric porous shell. Six models were built (two of which happen to be strictly identical, so were merged into one), leading to theoretical expressions for the longitudinal diffusion term in the van Deemter plate height equations of chromatographic columns. Three models were constructed by combining two effective diffusion models commonly used for binary composite media. Three other models were rigorously derived for ternary composite material. These models describe the physico-chemical problem of effective diffusion in ternary composite media and are based on either one or the combination of the following approaches: (1) the semi-empirical parallel diffusion model modified for diffusion hindrance caused by a nonporous solid core; (2) the effective medium theory of Landauer (binary and ternary composite materials); (3) the effective medium theory of Garnett with spherical inclusions (with one or two concentric; and (4) the probabilistic theory of effective conductivity elaborated by Torquato (binary only).

The most satisfactory results were obtained with the Garnett–Torquato model, which combines the Garnett diffusion model for a spherical non-porous core surrounded by a concentric shell (describing the exact geometry of a core–shell particle) and the Torquato diffusion model for a medium made of spheres in contact, dispersed in a homogeneous matrix (representing the random spatial distribution of spherical particles in a chromatographic column). The second most satisfactory model was obtained by solving the diffusion problem in a composite fractal material made exclusively of non-porous spheres surrounded by two concentric shells, which accounts for the porous stationary phase and the surrounding eluent in the packed column.

Calculations show that these two models are nearly equivalent for any value of the core-to-particle diameter ratio. The largest difference, $\Delta B = 0.18$, is observed for $\rho = 1$ when the impact of obstruction to diffusion caused by the solid core is largest.

The Landauer models fail to account for the $B$ coefficient of nonretained solutes because they do not account satisfactorily for the obstruction factor due to the solid particle-core. According to the Landauer theory, this coefficient should be smaller than 1.2 for $\rho > 0.80$ which is inconsistent with the results of the measurements of the actual obstruction factor ($B \simeq 1.2$) made by Knox [26], Tallarek [43], and Guiochon [37] with nonporous and randomly packed spherical particles. This result is not surprising because the effective medium theory of Landauer totally ignores the spatial arrangement of the different homogeneous phases in a composite material. Only the volume fractions of the phases matter, which, although important is insufficient to describe the actual diffusion problem in chromatographic columns.

Diffusion models based on the additivity of the diffusion fluxes in each homogeneous phase cannot predict the dependence of the $B$ coefficient on a wide range of $\rho$. They may occasionally provide values in satisfactory agreement with experimental results in a narrow range of $\rho$ but would fail in other ranges. Such models can be empirically completed by approximate obstruction factors $\gamma_e$ (diffusion in the mobile phase) and $\gamma_p$ (diffusion in the shell), in order to account for the experimental data for nonporous particles ($\rho = 1$). Experimental data are required to evaluate the limits of applicability of such semi-empirical models.

In a forthcoming paper, we will compare these theoretical results for $B(\rho)$ and experimental data measured by applying the peak parking method. We will report on the $B$ coefficients of the nonretained uracil ($k < 0.1$) and the strongly retained naphthalene ($k \simeq 5$) on four RPLC columns packed with shell particles having the same average diameter ($\simeq$1.7 μm) and different ratios $\rho$ (0.59, 0.70, 0.82, and 1.00). This comparison will allow the selection of the most accurate model of effective diffusion in packed chromatographic columns. Success in this endeavor would permit the accurate determination of the effective diffusion coefficients of a large variety of analytes (small and large molecular weight compounds), in different porous media. Parameters such as the internal obstruction factor of porous particles could become easily measurable.

## List of symbols

*Roman letters*

| | |
|---|---|
| $a_{bin}$ | parameter defined in Eq. (22) |
| $B$ | reduced longitudinal diffusion coefficient with reference to the interstitial linear velocity |
| $a_{ter}$ | parameter defined in Eq. (25) |
| $A_{i,k}$ | first integration constant related to the concentration profile in phase $i$ and to the Legendre polynomial of order $k$ (mol/m$^{3+k}$) |
| $B_{i,k}$ | second integration constant related to the concentration profile in phase $i$ and to the Legendre polynomial of order $k$ (mol/m$^{2-k}$) |
| $c_i$ | sample concentration in the homogeneous phase $i$ (mol/m$^3$) |
| $c_{eff}$ | average sample concentration in the composite material (mol/m$^3$) |
| $c_{core}$ | sample concentration in the core (mol/m$^3$) |
| $c_m$ | sample concentration in the bulk phase (mol/m$^3$) |
| $C_p$ | reduced trans-particle mass transfer coefficient with reference to the interstitial linear velocity |
| $c_{shell}$ | average sample concentration in the porous shell of the particle (mol/m$^3$) |
| $D_{app}$ | apparent axial diffusion coefficient of the sample in the column (m$^2$/s) |
| $d_c$ | inner diameter of the column stainless steel tube (m) |
| $D_{eff}$ | effective diffusion coefficient of the composite material (m$^2$/s) |
| $D_i$ | diffusion coefficient in the homogeneous phase $i$ (m$^2$/s) |
| $D_{core-shell}$ | effective diffusivity of the sample through the core–shell particle (m$^2$/s) |
| $D_m$ | bulk molecular diffusion coefficient (m$^2$/s) |
| $\vec{E}$ | opposite of the concentration gradient in the composite material (mol/m$^4$) |
| $E_0$ | uniform concentration gradient imposed to the composite material (mol/m$^4$) |
| $F_v$ | flow rate (m$^3$/s) |
| $\vec{j}_i$ | mass flux density in the homogeneous phase $i$ (mol/m$^2$/s) |
| $j_{shell}$ | mass flux density in the porous shell of the particle (mol/m$^2$/s) |
| $\vec{j}_{eff}$ | average mass flux density in the composite material (mol/m$^2$/s) |
| $K_1$ | equilibrium constant between phase 1 and phase 2 ($c_1/c_2$) |
| $K_2$ | equilibrium constant between phase 1 and phase 2 ($c_2/c_3$) |
| $K$ | equilibrium Henry's constant for the sample adsorption–desorption between the solid phase in the porous volume of the particle and the liquid eluent phase |
| $r$ | radial coordinate (m) |
| $r(\varphi)$ | radius of the core circle defined by the intersection of the $x$–$y$ plan and the spherical core surface (m) |
| $R(\varphi)$ | radius of the particle circle defined by the intersection of the $x$–$y$ plan and the spherical particle surface (m) |
| $r_1$ | radius of the non-porous core or homogeneous phase 1 (m) |
| $r_2$ | radius of the first concentric shell or homogeneous phase 2 (m) |
| $r_3$ | radius of the second concentric shell or homogeneous phase 3 (m) |
| $r_c$ | radius of the non-porous core (m) |
| $R_p$ | radius of the core–shell particle (m) |
| $t_p$ | parking time (s) |
| $\Delta t_p$ | increment of the peak parking time (s) |
| $u$ | interstitial linear velocity (m/s) |
| $z_i$ | location of the $x$–$y$ plan cut (m) |

*Greek letters*

| | |
|---|---|
| $\beta$ | parameter defined in Eq. (47) |
| $\Delta\sigma^2_{PP}$ | increment of the peak variance measure in the peak parking method (s$^2$) |
| $\epsilon_e$ | external column porosity |
| $\epsilon_p$ | particle porosity |
| $\epsilon_t$ | total column porosity |
| $\gamma$ | internal obstruction factor inside the porous shell |
| $\gamma_e$ | obstruction factor caused by randomly packed nonporous particles to the diffusion in the external bulk mobile phase |
| $\gamma_p$ | obstruction factor caused by a non-porous spherical core to the diffusion in the surrounding shell volume |
| $\gamma_2$ | obstruction factor caused by the geometry of phase 1 to the diffusion in phase 2 |
| $\gamma_3$ | obstruction factor caused by the geometry of phase 2 to the diffusion in phase 3 |
| $\Omega$ | ratio of the effective diffusivity of the sample in the porous shell to its bulk diffusion coefficient |
| $\phi_i$ | volume fraction of the homogeneous phase $i$ in the effective medium |
| $\rho$ | ratio of the solid non-porous core diameter to the core–shell particle diameter |

| | |
|---|---|
| $\rho(\varphi)$ | ratio of the core circle diameter $r(\varphi)$ to the particle circle diameter $R(\varphi)$ |
| $\sigma_i$ | electrical conductivity of the homogeneous phase $i$ (S/m) |
| $\sigma_{eff}$ | effctive electrical conductivity of the composite material (S/m) |
| $tau_p$ | tortuosity related to the diffusion in the porous shell surrounding a spherical non-porous core |
| $\theta$ | spherical angular coordinate |
| $\varphi$ | spherical angular coordinate |
| $\xi_2$ | three-point parameter for random dispersion of spherical inclusion |

## Acknowledgements

This work was supported in part by the cooperative agreement between the University of Tennessee and the Oak Ridge National Laboratory.

## References

[1] J.J. Kirkland, F.A. Truszkowski, C.H. Dilks, G.S. Engel, J. Chromatogr. A 890 (2000) 3.
[2] J.J. DeStefano, T.J. Langlois, J.J. Kirkland, J. Chromatogr. Sci. 46 (2007) 254.
[3] J.J. Kirkland, T.J. Langlois, J.J. DeStefano, Am. Lab. 39 (8) (2007) 18.
[4] S.A. Schuster, B. Wagner, B. Boyes, J. Kirkland, J. Chromatogr. Sci. 48 (2010) 566.
[5] F. Gritti, G. Guiochon, J. Chromatogr. A 1157 (2007) 289.
[6] A. Cavazzini, F. Gritti, K. Kaczmarski, N. Marchetti, G. Guiochon, Anal. Chem. 79 (2007) 5972.
[7] N. Marchetti, A. Cavazzini, F. Gritti, G. Guiochon, J. Chromatogr. A 1163 (2007) 203.
[8] F. Gritti, G. Guiochon, J. Chromatogr. A 1176 (2007) 107.
[9] D.V. McCalley, J. Chromatogr. A 1193 (2008) 85.
[10] F. Gritti, I. Leonardis, D. Shock, P. Stevenson, A. Shalliker, G. Guiochon, J. Chromatogr. A 1217 (2010) 1589.
[11] F. Gritti, G. Guiochon, J. Chromatogr. A 1217 (2010) 5069.
[12] F. Gritti, G. Guiochon, Chem. Eng. Sci. 65 (2010) 6310.
[13] F. Gritti, G. Guiochon, J. Chromatogr. A 1217 (2010) 1604.
[14] F. Gritti, C.A. Sanchez, T. Farkas, G. Guiochon, J. Chromatogr. A 1217 (2010) 3000.
[15] F. Gritti, I. Leonardis, J. Abia, G. Guiochon, J. Chromatogr. A 1217 (2010) 3819.
[16] E. Olh, S. Fekete, J. Fekete, K. Ganzler, J. Chromatogr. A 1217 (2010) 3642.
[17] F. Gritti, G. Guiochon, J. Chromatogr. A 1218 (2011) 907.
[18] F. Gritti, G. Guiochon, Chem. Eng. Sci. 65 (2010) 6327.
[19] F. Gritti, G. Guiochon, J. Chromatogr. A 1217 (2010) 8167.
[20] D.V. McCalley, J. Chromatogr. A 1217 (2010) 4561.
[21] J. Omamogho, J. Glennon, J. Hanrahan, J. Tobin, J. Chromatogr. A 1218 (2011) 1942.
[22] J.W. Jorgenson, L.E. Blue, E. Franklin, R.A. Lieberman, in: Presented at the Pittcon 2010 Conference, Orlando, FL, February 28–March 5, 2010, Paper 350-3.
[23] C. Horváth, S.R. Lipsky, J. Chromatogr. Sci. 7 (1969) 109.
[24] K. Kaczmarski, G. Guiochon, Anal. Chem. 79 (2008) 4648.
[25] A. Felinger, J. Chromatogr. A (2011), doi:10.1016/j.chroma.2010.10.025.
[26] J.H. Knox, L. McLaren, Anal. Chem. 36 (1964) 1477.
[27] G. Desmet, S. Deridder, J. Chromatogr. A 1218 (2011) 32.
[28] J.C. Giddings, Dynamics of Chromatography, Marcel Dekker, New York, NY, 1960.
[29] R. Landauer, J. Appl. Phys. 23 (1952) 779.
[30] H. Davis, J. Am. Ceram. Soc. 60 (1977) 499.
[31] J.C.M. Garnett, Philos. Trans. R. Soc. London, Ser. B 203 (1904) 385.
[32] S. Torquato, J. Appl. Phys. 58 (1985) 3790.
[33] S. Torquato, Random Heterogeneous Materials. Microstructure and Macroscopic Properties, Springer, New York, 2002.
[34] F. Gritti, G. Guiochon, AIChE J. 56 (2010) 1495.
[35] F. Gritti, G. Guiochon, J. Chromatogr. A 1217 (2010) 5137.
[36] F. Gritti, G. Guiochon, AIChE J. 57 (2011) 333.
[37] F. Gritti, G. Guiochon, AIChE J. 57 (2011) 346.
[38] H. Brenner, L. Gaydos, J. Colloid Interface Sci. 58 (1977) 312.
[39] F. Gritti, G. Guiochon, Anal. Chem. 78 (2006) 5329.
[40] C. Wilke, P. Chang, AIChE J. 1 (1955) 264.
[41] F. Gritti, G. Guiochon, J. Chromatogr. A, submitted for publication.
[42] F. Gritti, G. Guiochon, Chem. Eng. Sci. 61 (2006) 7636.
[43] F.C. Leinweber, U. Tallarek, J. Chromatogr. A 1006 (2003) 207.